HHS Public Access

Author manuscript

J Am Chem Soc. Author manuscript; available in PMC 2018 October 30.

Published in final edited form as:

J Am Chem Soc. 2018 September 12; 140(36): 11153–11157. doi:10.1021/jacs.8b05780.

Methane Storage in Paddlewheel-Based Porous Coordination Cages

Casey A. Rowland[†], **Gregory R. Lorzing**[#†,‡], **Eric J. Gosselin**[#†,‡], **Benjamin A. Trump**[#‖], **Glenn P. A. Yap**[†], **Craig M. Brown**[§,‖], and **Eric D. Bloch**[*,†,‡]

[†]Department of Chemistry and Biochemistry, University of Delaware, Newark, Delaware 19716 United States

[‡]Center for Neutron Science, University of Delaware, Newark, Delaware 19716 United States

[§]Department of Chemical and Biomolecular Engineering, University of Delaware, Newark, Delaware 19716 United States

[‖]Center for Neutron Research, National Institute of Standards and Technology, Gaithersburg, Maryland 20899, United States

[#] These authors contributed equally to this work.

Abstract

Although gas adsorption properties of extended three-dimensional metal−organic materials have been widely studied, they remain relatively unexplored in porous molecular systems. This is particularly the case for porous coordination cages for which surface areas are typically not reported. Herein, we report the synthesis, characterization, activation, and gas adsorption properties of a family of carbazole-based cages. The chromium analog displays a coordination cage record BET (Brunauer−Emmett−Teller) surface area of 1235 m^2/g. With precise synthesis and activation procedures, two previously reported cages similarly display high surface areas. The materials exhibit high methane adsorption capacities at 65 bar with the chromium (II) cage

[*]Corresponding Author edb@udel.edu.

ASSOCIATED CONTENT

Supporting Information

The Supporting Information is available free of charge on the ACS Publications website at DOI: 10.1021/jacs.8b05780.

Detailed experimental procedures, powder X-ray and neutron diffraction data, gas adsorption isotherms and fits, and spectroscopic data (PDF)

Single-crystal data for $C_{204}H_{176}Cu_{12}N_{24}O_{66}$ (CIF)

Single-crystal data for $C_{210}H_{178}Cr_{12}N_{26}O_{68}$ (CIF)

Single-crystal data for $C_{168}H_{84}Mo_{12}N_{12}O_{68}$ (CIF)

Single-crystal data for $C_{17.00}CuH_{8.00}NO_4$ (CIF)

Single-crystal data for $C_{17.79}H_{8.00}CuD_{3.17}NO_4$ (CIF)

Single-crystal data for $C_{18.89}H_{8.00}CuD_{7.56}NO_4$ (CIF)

Single-crystal data for $C_{20.25}H_{8.00}CuD_{13.00}NO_4$ (CIF)

Notes

The authors declare no competing financial interest.

displaying CH_4 capacities of 194 cm^3/g and 148 cm^3/cm^3. This high uptake is a result of optimal pore design, which was confirmed via powder neutron diffraction experiments.

As a result of continually increasing global reserves,[1] natural gas has been touted as a cleaner alternative to gasoline and coal as a fuel in the transportation and power generation sectors, respectively.[2,3] Because natural gas primarily consists of methane, which is the upper limit of H:C ratio, it is the most gravimetrically energy dense hydrocarbon fuel. Consequently, its combustion releases considerably less pollutants on a per energy basis.[4] Indeed, U.S. CO_2 emissions from power generation are near a 30 year low resulting from a transition to natural gas.[5] In the transportation sector, however, the low volumetric energy density of methane at STP has limited its utility.[6] Proposed solutions to this have included liquefaction or compression. Both of these have generally been viewed as not viable in passenger vehicles.[7] Adsorbed natural gas systems have shown promise in this regard.[8] The challenge here is the development of an adsorbent with appropriate methane capacity. Zeolites,[9,10] activated carbons,[11] metal−organic frameworks (MOFs),[12–18] and a variety of other porous materials have been investigated for high pressure natural gas storage. MOFs currently display the most promising uptakes[19–22] with reported CH_4 adsorption capacities as high as 259 cm^3/cm^3.[23] Additionally, a number of interesting adsorption properties have been observed in these materials, including flexibility for thermal management and temperature-dependent negative gas adsorption.[22,24] However, advancements in this area remain short of Department of Energy targets.[25]

Porous molecular adsorbents may show promise in this regard as they can be thought of as soluble adsorbents with designer pores. This could potentially endow them with favorable properties such as tailored syntheses, flexibility upon adsorption, cooperative binding, and increased ease of processability. These molecules, which can be either all-organic[26–28] or metal−organic,[29–31] are discrete zero-dimensional materials that display permanent porosity in the solid state. Although the underlying chemistry of porous organic cages and porous coordination cages has been established for decades, permanent porosity in these materials is a relatively recent phenomena when compared to zeolites and MOFs. As a result, they have remained almost completely unexplored for high-pressure gas storage applications. This is somewhat surprising given their conceptually analogous nature to porous extended solid materials. In fact, many metal−organic frameworks contain cages as their building units.[32,33] In an effort to expand the library of carboxylate-based porous cages, we have thoroughly investigated the synthesis of novel isophthalic acid and carbazole-dicarboxylic acid materials.[34] These latter molecules are particularly interesting for gas storage applications as the $M_{12}(cdc)_{12}$ (cdc^{2-} = carbazoledi-carboxylic acid) octahedral cage is present as one of three cages in DUT-49[20] and PCN-82,[35] two MOFs with high methane and hydrogen storage capacities, respectively. Given the high surface area of recently reported cuboctahedral $M_{24}(R\text{-}bdc)_{24}$ cages based on chromium(II),[30,36] we sought to expand the synthesis of $M_{12}(cdc)_{12}$ to this metal as a porous cage of this type is expected to show promising high-pressure adsorption properties.

Analogous to the synthesis of the Cu- and Mo-based $M_{12}(cdc)_{12}$ materials, the air-free reaction of anhydrous $Cr_2(OAc)_4$ with H_2cdc in a dimethylformamide (DMF)/methanol

(MeOH) mixture affords $Cr_{12}(cdc)_{12}\cdot n$DMF as large red/purple crystals. Single crystal X-ray diffraction confirms the material is isostructural to the previously reported Cu^{2+} and Mo^{2+} cages.[37,38] This structure is comprised of six bimetallic paddlewheel units in an octahedral arrangement coordinated to 12 cdc^{2-} ligands (Figure 1). The cages consist of 8 triangular windows with corner−corner distances of approximately 12 Å. The molecules pack in the solid state with cage center to center distances of approximately 22 Å. The structure of $Cr_{12}(cdc)_{12}$ contains solvent accessible voids in excess of 60%, which rivals the values displayed by many MOFs. Accordingly, thermogravimetric analysis (TGA) of a DMF-exchanged sample reveals a mass loss of 40% at 250 °C (Figure S4). Precise solvent exchange protocols must be implemented to achieve high surface areas for molecular materials as cages are potentially soluble in a variety of solvents. For $Cr_{12}(cdc)_{12}$, room temperature solvent exchanges with DMF and methanol were used. Powder X-ray diffraction confirms the as-synthesized material retains high crystallinity upon exchange with DMF and methanol (Figure 2). However, given the lack of three-dimensional connectivity and in contrast to most MOFs, there is significant structural rearrangement upon initial solvent exchange. Activation at 70 °C affords a BET surface area of 1235 m^2/g. To the best of our knowledge, this is the highest surface area reported for a molecular metal −organic material.

In order to achieve comparable surface areas for $Cu_{12}(cdc)_{12}$ and $Mo_{12}(cdc)_{12}$, we surveyed a range of synthesis, solvent exchange, and activation procedures. In contrast to metal−organic frameworks where identical surface areas for a material should be obtained regardless of synthesis conditions (assuming phase purity and full activation), a porous coordination cage can deposit in different crystalline phases depending on synthetic conditions. Although the individual cage structures remain in these various analogs, their three-dimensional packing, stability, and porosity can potentially vary. For $Mo_{12}(cdc)_{12}$, a DMPU-based synthesis was reported affording a solid that crystallizes in $R\bar{3}$.[38] Despite our best efforts, we were only able to obtain an activated material with a surface area of approximately 550 m^2/g. Synthesis of the cage in DEF affords the same cage that instead crystallizes in $P2_1/n$. Methanol exchange of this material followed by activation at 50 °C affords a solid with a BET surface area of 1108 m^2/g. In an analogous manner, $Cu_{12}(cdc)_{12}$ can be synthesized and crystallized from a variety of amide-based solvents. The highest surface area that was observed (657 m^2/g) was for a material synthesized in DMF/MeOH, washed in MeOH, and activated at 50 °C.

To evaluate the methane storage potential of the three porous cages, high-pressure adsorption isotherms were collected from 0 to 65 bar at 298 K. At 35 bar the total gravimetric uptakes follow the surface area trends with capacities of 148, 135, and 81 cm^3/g for $Cr_{12}(cdc)_{12}$, $Mo_{12}(cdc)_{12}$, and $Cu_{12}(cdc)_{12}$, respectively (Figure 3). These values are not only significantly higher than those for previously reported coordination cages,[39] they are consistent with the capacities displayed by metal−organic frameworks with similar surface areas.[15] Methane uptake increases up to at least 65 bar with the $Cr_{12}(cdc)_{12}$ displaying the highest gravimetric capacity of 194 cm^3/g while $Mo_{12}(cdc)_{12}$ has the highest volumetric capacity (150 cm^3/cm^3) (Table 1) (Figures S30, S31). To the best of our knowledge, both the gravimetric and volumetric capacities are the highest observed for a porous molecular

assembly. For all three materials, moderate hysteresis is seen upon desorption, likely a result of the lack of three-dimensional connectivity between the cages.

To directly compare the CH_4 storage capacities of $M_{12}(cdc)_{12}$ cages with MOFs containing similar methane binding environments, we targeted previously reported materials with $M_{12}(cdc)_{12}$ as their building units. DUT-49 has been thoroughly investigated for its high CH_4 uptake at high pressure, however the flexibility of the material complicates adsorption studies.[24] Two analogous materials, PCN-81 and PCN-82, are similarly based on $M_{12}(cdc)_{12}$ cages, although the former was shown to lack permanent porosity.[35] However, synthesis of PCN-81 via the reported route followed by thorough room temperature DMF and MeOH exchanges and activation at 100 °C afforded a highly crystalline material with a BET surface area of 4050 m^2/g. Consistent with its high gravimetric surface area, PCN-81 displays an incredibly high CH_4 uptake of 305 cm^3/g at 35 bar and 298 K. At 65 bar this value reaches 449 cm^3/g. Given the low density of the material, its volumetric capacity at 35 bar is significantly lower at 147 cm^3/cm^3. As a result of the shallow nature of its adsorption isotherm (Figure 3), PCN-81 has a deliverable CH_4 capacity of 190 cm^3/cm^3 for a pressure swing of 65 to 5 bar, which is on par with the highest value reported for a porous material. Low temperature isotherms collected over a range of temperatures indicate methane adsorption enthalpies of −16 to −18.5 kJ/ mol for all four materials.

We turned to powder neutron diffraction to gain insight into the nature of CH_4 adsorption in these materials. Although the porous coordination cages retain crystallinity upon solvent removal, it is decreased during activation to the point of precluding the use of diffraction studies to interrogate binding sites. PCN-81, however, remains highly crystalline upon degassing. Refinement of data collected on an activated sample reveals it is significantly less distorted upon evacuation (Figure 4) compared to its solvated state.[35] At a CD_4:Cu loading of 1:1, three main adsorption sites are apparent. Although the framework is composed of three types of pores, the methane is exclusively adsorbed in the $M_{12}(cdc)_{12}$ cage. A primary adsorption site is the open copper(II) center with a Cu−C distance of 2.777(5) Å and an occupancy of 0.63(3). A site with similar occupancy (0.64(3)) is at the edge of a carbazole ligand with $C_{methane}$−C_{ligand} distances of 3.27 and 3.69 Å. This methane molecule is only present in six of the eight triangular windows of the $Cu_{12}(cdc)_{12}$ building unit. Together, these two adsorption sites form the basis for the lowest occupancy site (0.28(3)) in a triangular pocket between two of the metal-bound CD_4 and a carbazole-bound CD_4 with methane−methane distances of 2.79−4.13 Å (Figure 4). At double the methane loading, a number of additional sites are populated. The occupancy of the first two sites are essentially unchanged while the occupancy of the third site increases to 0.37(3). At this loading, the final two triangular windows of the cage are populated at their three corners. An additional adsorption site on the inside of the cage and the copper on the exterior bind methane at this loading. Increasing the methane dose to 4.0/ Cu reveals no additional CD_4 binding sites, although the overall occupancy increases. Interestingly, at this loading the small cage in PCN-81 remains the only one that is occupied. Furthermore, the concurrent population of multiple adsorption sites in PCN-81 is consistent with the shallow nature of the adsorption isotherm, which indicates a lack of very strong methane binding sites. Eight methane adsorption sites are related by symmetry to afford a total methane capacity of 49 molecules per cage. This corresponds to a methane adsorption capacity of approximately 260 cm^3/g, a

value PCN-81 reaches by 35 bar. At this pressure, the two additional pores in the material remain unoccupied but would allow for additional storage at higher pressures. At lower pressures, the two other pores are essentially empty space that is detrimental to the density, and thus volumetric capacity of the material. This is consistent with the nearly equal volumetric adsorption capacities of PCN-81, $Cr_{12}(cdc)_{12}$, and $Mo_{12}(cdc)_{12}$ at 35 bar and 298 K.

In conclusion, we have shown that with precise synthesis, solvent exchange, and activation procedures, high surface areas are attainable for porous coordination assemblies. Although the surface areas displayed by these materials currently fall short of the record values displayed by metal−organic frameworks, the materials discussed here show the potential utility of porous coordination cages for high-pressure gas storage. Neutron diffraction experiments suggest the $M_{12}(cdc)_{12}$ cage that is also present in PCN-81 and a number of related MOFs may be the optimal pore environment for high-pressure methane storage. An ideal methane storage material may consist nearly entirely of $M_{12}(cdc)_{12}$ cages, whether it is molecular or an extended solid. Future work along these lines will involve tailoring cage stability, solubility, and gas uptake via ligand functionalization.

Supplementary Material

Refer to Web version on PubMed Central for supplementary material.

Acknowledgments

Funding

We are grateful to the University of Delaware for start-up funds. This paper was prepared under cooperative agreement no. 70NANB17H302 from NIST, U.S. Department of Commerce. We acknowledge the support of the National Institute of Standards and Technology, U.S. Department of Commerce, in providing the neutron facilities used in this work. This research used resources of the Advanced Photon Source, a U.S. Department of Energy (DOE) Office of Science User Facility operated for the DOE Office of Science by Argonne National Laboratory under Contract No. DE-AC02-06CH11357. We thank the staff of 17-BM for help with synchrotron X-ray data collection. B.A.T. recognizes the National Academies/National Research Council for his Postdoctoral Fellowship. A portion of this work was supported by the National Institutes of Health under award number P20GM104316. The content is solely the responsibility of the authors and does not necessarily represent the official views of the National Institutes of Health.

REFERENCES

(1). Xu C; Bell L Oil 2017, 115, 18–19.

(2). Khan MI Energy Policy 2017, 110, 126–136.

(3). Pratson LF; Haerer D; Patino-Echeverri D Environ. Sci. Technol 2013, 47, 4926–4933. [PubMed: 23496173]

(4). Celzard A; Fierro V Energy Fuels 2005, 19, 573–583.

(5). Annual Energy Outlook 2018 U.S. Energy Information Administration, www.eia.gov/aeo (accessed 05/31/2018).

(6). Alternative Fuels Data Center − Fuel Properties Comparison, 2013, http://www.afdc.energy.gov/fuels/fuel_comparison_chart.pdf. (accessed 05/31/2018).

(7). Rios-Mercado RZ; Borraz-Sanchez C Appl. Energy 2015, 147, 536–555.

(8). Vasiliev LL; Kanonckik LE; Mishkinis DA; Rabetsky MIInt. J. Therm. Sci 2000, 39, 1047–1055.

(9). Duren T; Sarkisov L; Yaghi OM; Snurr RQ Langmuir 2004, 20, 2683–2689. [PubMed: 15835137]

(10). Menon VC; Komarneni SJ Porous Mater 1998, 5, 43–58.

(11). Lozano-Castello D; Alcaniz-Monge J; de la Casa-Lillo MA;Cazorla-Amoros D; Linares-Solano A Fuel 2002, 81, 1777–1803.

(12). Furukawa H; Yaghi OM J. Am. Chem. Soc 2009, 131, 8875– 8883. [PubMed: 19496589]

(13). Ma S; Zhou HC Chem. Commun 2010, 46, 44–53.

(14). Makal TA; Li J-R; Lu W; Zhou H-C Chem. Soc. Rev2012, 41, 7761–7779. [PubMed: 22990753]

(15). Mason JA; Veenstra M; Long JR Chem. Sci 2014, 5, 32– 51.

(16). He Y; Qian G; Chen B; Zhou W Chem. Soc. Rev 2014, 43, 5657–5678. [PubMed: 24658531]

(17). Li B; Wen H-M; Zhou W; Xu JQ; Chen C Chem 2016,1, 557–580.

(18). Lin Y; Kong C; Zhang Q; Chen L Adv. Energy Mater 2017,7, 1601296.

(19). Ma S; Sun D; Simmons JM; Collier CD; Yuan D; Zhou H-CJ Am. Chem. Soc 2008, 130, 1012–1016.

(20). Stoeck U; Krause S; Bon V; Senkovska I; Kaskel S Chem. Commun 2012, 48, 10841–10843.

(21). Gandara F; Furukawa H; Lee S; Yaghi OM J. Am. Chem. Soc 2014, 136, 5271–5274. [PubMed: 24661065]

(22). Mason JA; Oktawiec J; Taylor MK; Hudson MR;Rodriguez J; Bachman JE; Gonzalez MI; Cervellino A; Guagliardi A; Brown CM; Llewellyn PL; Masciocchi N; Long JR Nature 2015, 527, 357–361. [PubMed: 26503057]

(23). Tian T; Zeng Z; Vulpe D; Casco ME; Divitini G;Midgley PA; Silvestre-Albero J; Tan J-C; Moghadam PZ; Fairen-Jimenez D Nat. Mater 2018, 17, 174–179. [PubMed: 29251723]

(24). Krause S; Bon V; Senkovska I; Stoeck U; Wallacher D;Tobbens DM; Zander S; Pillai RS; Maurin G; Coudert F-X; Kaskel S Nature 2016, 532, 348–352. [PubMed: 27049950]

(25). Methane Opportunities for Vehicular Energy; Funding Opportunity no. DE-FOA-0000672; Advanced Research Project Agency− Energy, U.S. Department of Energy, 2012.

(26). Tozawa T; Jones JTA; Swamy SI; Jiang S; Adams DJ; Shakespeare S; Clowes R; Bradshaw D; Hasell T; Chong SY; Tang C; Thompson S; Parker J; Trewin A; Bacsa J; Slawin AMZ; Steiner A; Cooper AI Nat. Mater 2009, 8, 973–978. [PubMed: 19855385]

(27). Chen L; Reiss PS; Chong SY; Holden D; Jelfs KE;Hasell T; Little MA; Kewley A; Briggs ME; Stephenson A; Thomas KM; Armstrong JA; Bell J; Busto J; Noel R; Liu J; Strachan DM; Thallapally BK; Cooper AI Nat. Mater 2014, 13, 954–960. [PubMed: 25038731]

(28). Hasell T; Cooper AI Nat. Rev. Mater 2016, 1, 16053.

(29). Chen T-H; Wang L; Trueblood JV; Grassian VH; Cohen SM J. Am. Chem. Soc 2016, 138, 9646–9654. [PubMed: 27400759]

(30). Lorzing GR; Trump BA; Brown CM; Bloch ED Chem.Mater 2017, 29, 8583–8587.

(31). Fang Y; Xiao Z; Li J; Lollar C; Liu L; Lian X; Yuan S;Banerjee S; Zhang P; Zhou H-C Angew. Chem., Int. Ed 2018, 57, 5283–5287.

(32). Yan Y; Lin X; Yang S; Blake AJ; Dailly A; Champness NR; Hubberstey P; Schroder M Chem. Commun 2009, 0, 1025– 1027.

(33). Wu H; Simmons JM; Liu Y; Brown CM; Wang X-S; Ma S; Peterson VK; Southon PD; Kepert CJ; Zhou H-C; Yildirim T; Zhou W Chem. Eur. J 2010, 16, 5205–5214. [PubMed: 20358553]

(34). Gosselin EJ; Rowland CA; Balto KP; Yap GPA;Bloch ED Design and Synthesis of Porous Nickel(II) and Cobalt(II) Cages. Inorg. Chem 2018, DOI: DOI: 10.1021/acs.inorgchem.8b01130.

(35). Lu W; Yuan D; Makal TA; Wei Z; Li J-R; Zhou H-C Dalton Trans 2013, 42, 1708–1714. [PubMed: 23160711]

(36). Park J; Perry Z; Chen Y-P; Bae J; Zhou H-C ACS Appl. Mater. Interfaces 2017, 9, 28064–28068. [PubMed: 28741931]

(37). Li J-R; Timmons DJ; Zhou H-CJ Am. Chem. Soc 2009,131, 6368–6369.

(38). Li J-R; Yakovenko AA; Lu W; Timmons DJ; Zhuang W; Yuan D; Zhou H-CJ Am. Chem. Soc 2010, 132, 17599– 17610.

(39). Sudik AC; Millward AR; Ockwig NW; Cote AP; Kim J;Yaghi OM J. Am. Chem. Soc 2005, 127, 7110–7118. [PubMed: 15884953]

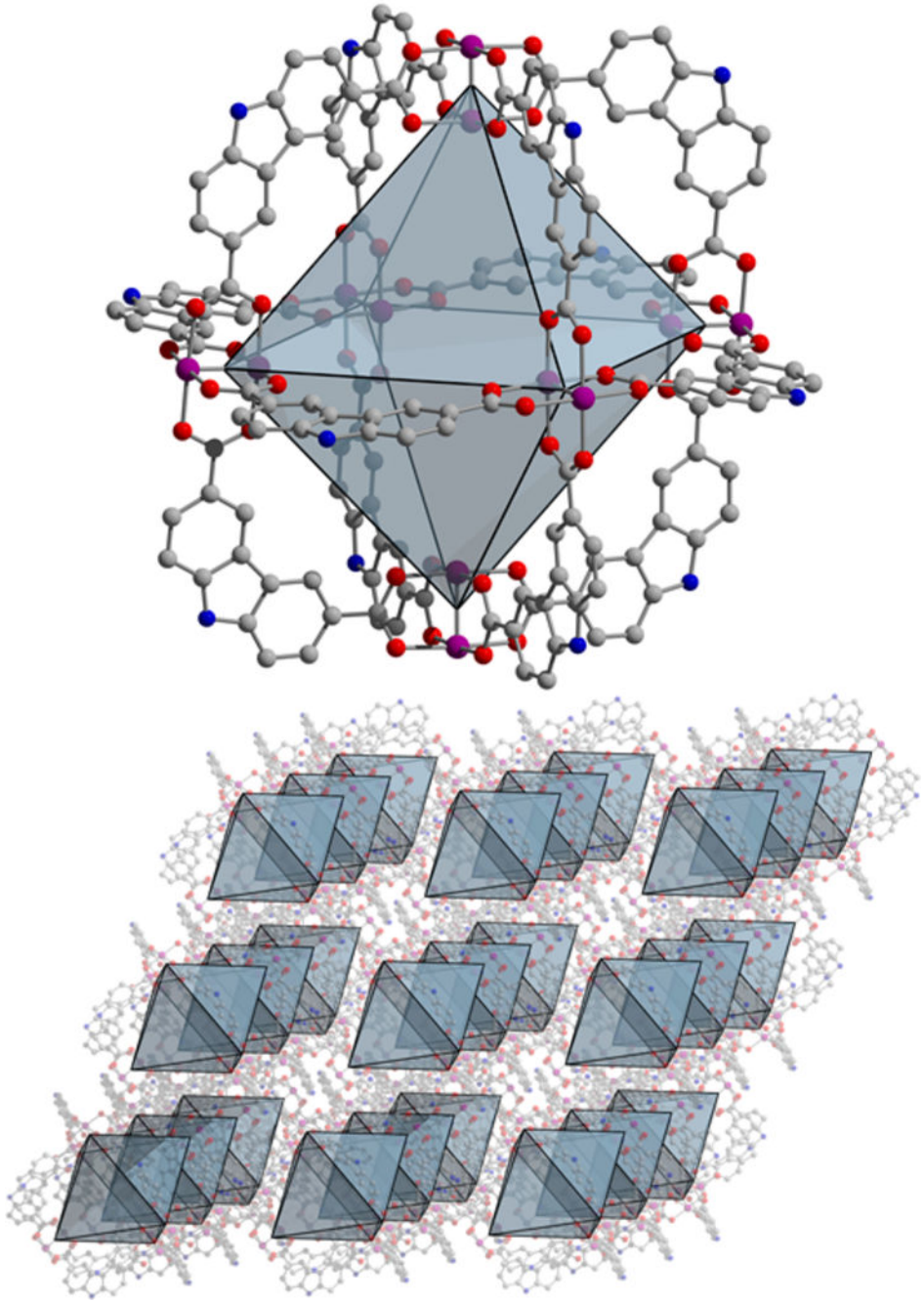

Figure 1.

Structure of $Cr_{12}(cdc)_{12}$ as determined by single-crystal X-ray diffraction. Purple, gray, red, and blue represent chromium, carbon, oxygen, and nitrogen, respectively. Hydrogen atoms and solvent molecules have been omitted.

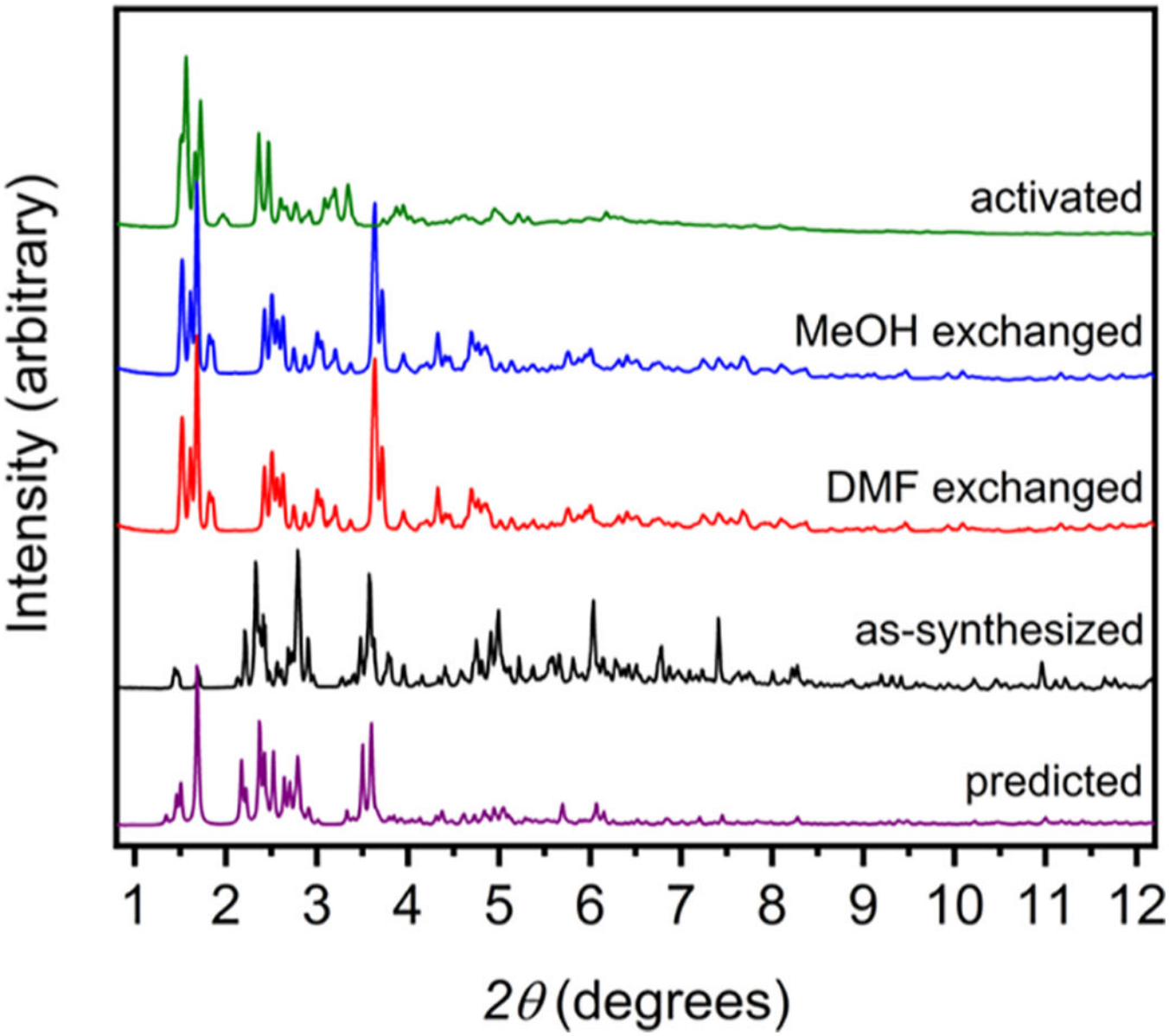

Figure 2.
Powder X-ray diffraction patterns of as-synthesized (black), DMF exchanged (red), MeOH exchanged (blue), and desolvated (green) $Cr_{12}(cdc)_{12}$ vs predicted (purple).

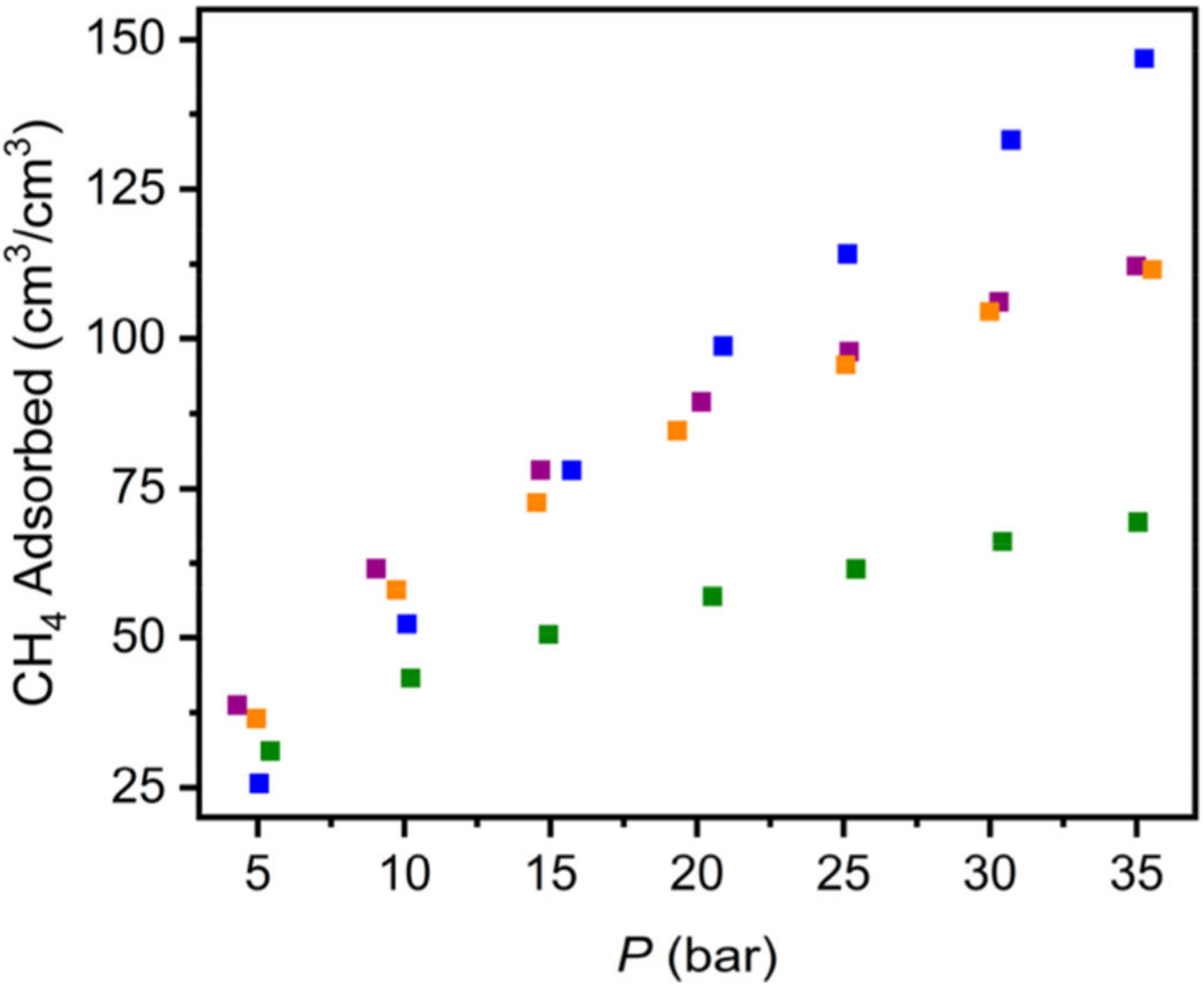

Figure 3.

Total high-pressure CH_4 adsorption at 298 K in $Cr_{12}(cdc)_{12}$ (purple), $Mo_{12}(cdc)_{12}$ (orange), $Cu_{12}(cdc)_{12}$ (green), and PCN-81 (blue).

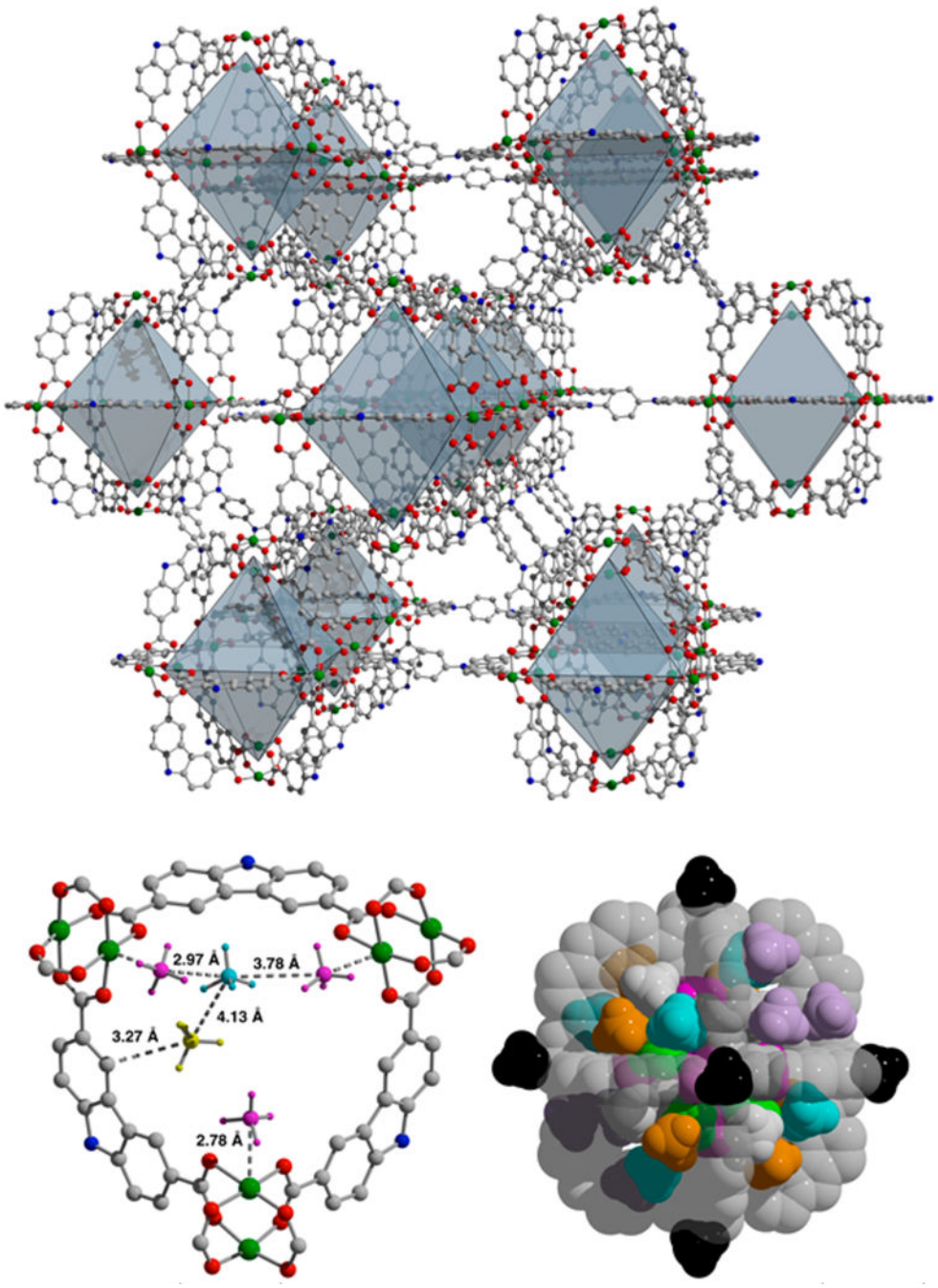

Figure 4.

(Upper) Structure of activated PCN-81. (Lower) CD_4 adsorption in PCN-81 as determined by powder neutron diffraction. (Left) At low loading three sites in the $Cu_{12}(cdc)_{12}$ portion of the structure are populated. (Right) Up to 4.0 CD_4/Cu, methane exclusively resides in the octahedral cage. With 12 Cu^{2+} ions per cage, this results in a cage capacity of 49 methane molecules.

Table 1.

Methane Storage Properties of $M_{12}(cdc)_{12}$ Cages in Comparison to PCN-81, HKUST-1, and IRMOP-51[a]

Material	BET Surface Area m^2/g	35 bar Capacity cm^3/g [cm^3/cm^3]	65 bar Capacity cm^3/g [cm^3/cm^3]
IRMOP-51[39]	480	48.4 [25]	—
$Cu_{12}(cdc)_{12}$	657	81.3 [69.4]	111.8 [95.4]
$Cr_{12}(cdc)_{12}$	1235	147.5 [112.1]	193.9 [147.8]
$Mo_{12}(cdc)_{12}$	1108	135.0 [111.5]	181.1 [150.0]
PCN-81	4050	305.3 [146.8]	448.7 [215.8]
HKUST-1[15]	1850	255.24 [224.9]	298.5 [263.0]

[a]All values are total uptake.